



Research Article

ISSN : 2277-3657
CODEN(USA) : IJPRPM

Prostatic Histopathologic and Electron Microscopic Changes Following Intraperitoneal Injection of Gold Nanorods to Male Albino Rats

Mahmoud A. A. Said^{1*}, Ahmed Sabry S. Abdoon², Sayed A. Aziz¹, Gamal Shams¹, Sayed R. Elattar³, Sameh M. El Nabtity³

¹ Department of Pharmacology, Faculty of Veterinary Medicine, Zagazig Univeristy, Egypt

² Department of Animal Reproduction, Veterinary Research Division, National Research Centre, Dokki 12622, Cairo, Egypt

³ Department of Pathology, Faculty of Veterinary Medicine, Zagazig Univeristy, Egypt.

***Corresponding Author Email:** ph.mahmoud.91@gmail.com

ABSTRACT

The field of nanomedicine has been developed to achieve enhanced and targeted delivery of biomolecules including nanoparticles. Despite their convenience, metal nanoparticles confront strenuous challenges including toxicity, low translocation ability into cells and clearance from the organs. This study aims to detect the *in vivo* cellular interaction between prostatic tissues and gold nanorods on the prostatic tissue and to detect the short-term effect of the gold nanorods to reach prostatic tissue by histopathologic and electron microscopic examinations. Forty-eight adult male albino rats (180-200 g) were used. They were divided into 2 equal groups. The 1st group received injection of saline 0.9% (i.P); while, the 2nd group received 1 ml of 300 µg/kg body weight of AuNRs. On days 1, 3, 7, and 14 post-treatment, six animals from each group were sacrificed and the prostate was dissected and cut into two sections for performing histopathologic and EM study. It has been found that the short term effect of gold nanorods induced pyknotic and apoptotic changes as well as presence of phagocytosis in the prostate tissues. From this study, it could be concluded that gold nanorods have reached prostate tissue; therefore, it could be helpful in upcoming days to establish a concept on the role of gold nanorods in the management of cellular biological behaviors.

Key words: Gold Nanorods, Male Albino Rats, Electron Microscope, Prostate.

INTRODUCTION

An approximate number of 10,000 publications are published per year, though the term “Nanomedicine” only appeared at the turn of this century [1]. Nanomedicine applications trace back to the use of colloidal gold long ago, but Metchnikov and Ehrlich are the modern developers of nanomedicine for their research efforts and works on phagocytosis. Not all drugs are hydrophilic and this could be a dilemma. To overcome this disadvantage, nanocarriers like polymer nanocapsules, polymer-protein conjugates, albumin-drug conjugates, block-copolymer micelles, anti-arthritis gold nanoparticles and anti-microbial silver nanoparticles have been designed to be hydrophilic. Although these nanovectors are designed to pass through the gastro-intestinal tract, lung, and blood-brain barriers, the amount of drug that reaches the target organ is lower than 1% [2].

Nowadays, the field of nanomedicine has been developed to enhance the targeted drug delivery including metal nanoparticles. Even though this type of nanoparticles is convenient, they are hazardous. This in turn can induce toxicity, inefficient translocation into cells and clearance from tissues or organs. These barriers can be broken by functionalization of gold nanoparticles (AuNPs) with poly ethylene glycol (PEG). This type of nanoparticles has exhibited low cytotoxicity and excellent bio-distribution abilities [3]. These functionalized AuNPs can be used for gene transfection and silencing, targeted drug or gene delivery [4]. Gold nanorods are one of the forms of gold nanoparticles that are featured by their good penetrating ability and tissue uptake [5]. It is essential to understand the short term effect of gold nanorods through its *in vivo* biological interaction. Our study is

focused on the penetrating ability of Gold nanorods (GNRs) to normal prostate. The aim of this study is to evaluate the possibility of gold nanorods to induce histopathological and electron microscopic alterations to normal prostate tissue, detect the intensity of the induced alteration, and establish a concept on the role of gold nanorods in the upcoming studies related to cellular biological behaviors.

MATERIAL AND METHODS

Chloroauric acid ($\text{HAuCl}_4 \cdot \text{H}_2\text{O}$), Cetyltrimethylammonium bromide (CTAB), ascorbic acid and sodium borohydride (NaBH_4) were the purchases made from Sigma-Aldrich Co. Deionized water (Milli-Q water) was used to prepare all the solutions.

Synthesis of gold nanorods (GNRs)

Using the seed-growth approach based on the method by Nikoobakht and El-Sayed (2003), a solution was prepared containing GNRs [6]. Briefly, the following steps were performed to carry out the reaction: 1) Seeding solution: 5 mL of (5×10^{-4} M) HAuCl_4 was added to CTAB solution (5 mL, 2×10^{-1} M) with gentle shaking and an orange solution was obtained. 600 μL of (10^{-2} M) ice-cold NaBH_4 was added at once to the above mixture. The color of the mixture was instantly turned from orange to reddish brown. 2) Growth solution: 300 μL of (4×10^{-3} M) AgNO_3 was added to a mixture of CTAB (5 mL, 2×10^{-1} M). Then, 70 μL of (7.8×10^{-2} M) ascorbic acid was added to this aqueous mixture resulting in color change from orange to colorless. Finally, an injection was done to the growth solution containing 12 μL seed solution and accordingly, a change was appeared with regard to the color of the growth solution within 30-45 min to reddish purple. 3) Gold Nanorods PEGylation: Thiol-terminated methoxypoly-(ethylene glycol) (mPEG-SH) (MW=5000) was a purchase made from Nanocs Co. Centrifuge of the raw nanorods solution was done for 20 min at 15000 rpm in order to pellet the nanorods; then, it was decanted, and re-suspended to 10 ml of deionized water aimed at removing the excess CTAB. To the nanorods solution, 0.05 g of mPEG-SH was added. At room temperature condition, the mixture was kept overnight, then centrifuged, decanted, and re-suspended twice in deionized water in order to remove the excess CTAB as well as mPEG-SH.

Characterization of GNRs

Spectrophotometer (Japan) recorded the absorption spectra of GNRs solutions. A strong absorption band (~ 700 nm) which was resulted from the electronic oscillation of the electrons of the nanorod along its long axis and a weak band (~ 500 nm) polarized along the short axis which was resulted from nanorod electrons oscillations along the short axis of the gold nanorod. JEOL JEM 2010 TEM operated at 100 kV accelerating voltage was used to obtain the transmission electron microscopic (TEM) images. According to the TEM results, most of the nanoparticles are rod shaped with the long to the short axis length ratio of ~ 4 . Accordingly, they absorb the light at ~ 700 nm (near infrared light) which is not true for the other spheres or shapes that are not capable of absorbing the near infrared light used and based on the mentioned factors, they will not get hot to kill the cancer cells.

Animals and experimental design

An ethical approval was obtained from IACUC committee of Zagazig University, Egypt with the code number of ZU-IACUC/2/F/49/2018.

In this study, forty-eight 180-200 gm adult male Albino rats Wistar strain were used which were provided by the Animal House laboratory at Faculty of Veterinary Medicine, Zagazig University. They were left for a one-week period for acclimatization. They were fed on balanced ration and water was added ad libitum. The rats were divided into two equal groups. The first group was injected with 1 ml normal saline 0.9% intraperitoneally and kept as a control group; while, the second group received 1 ml of 300g AuNRs/kg body weight intraperitoneally as one shot¹. On Days 1, 3, 7 and 14 post-treatment, six animals from each group were sacrificed and the prostate gland was dissected. Prostate tissues were cut into two parts. The first portion was kept in jar containing 10% buffered formalin for histopathological examination; while, the second portion was kept in a jar containing 2.5% glutraldehyde for electron microscopic examination.

Histopathological study:

The formalin preserved prostate tissues and they were processed in an automated tissue processor that the processing contained an initial 2-step fixation and dehydration. Fixation was comprised of tissue immersion in 10% buffered formalin for 48 hours, followed by removal of preservative in distilled water for 30 minutes.

¹ Zhang, et al., (2010) attached IL-2 and anti- D137 on the surface of liposomes to allow these immune mediators to rapidly target and accumulate in tumor with low risk of systemic exposure and toxicity.

Then, by running the tissues through a graded series of alcohol (70%, 90% and 100%), dehydration was carried out. The tissue was exposed to 70% and 90% alcohol for 120 and 90 minutes, respectively and then exposed to two cycles of absolute alcohol, each for one hour. Dehydration was then followed by clearing the samples in several changes of xylene. The samples were filled with molten paraffin wax, then embedded and blocked out. Paraffin sections (4–5 μ m) were stained with hematoxylin and eosin [7]. The stained sections were examined for inflammatory reactions, degenerative, necrotic, apoptotic changes and any other pathological lesions in the examined prostate tissues of experimental rats.

Transmission Electron Microscopy (TEM):

The stained sections were examined with a JEOL 1010 Transmission Electron Microscope at the Regional Center for Mycology and Biotechnology (RCMB), Al-Azhar University. Specimen tissues were prepared for TEM according to John J et al. (1999) [8].

RESULTS

AuNRs preparation and characterization

TEM image of the prepared AuNRs is presented in Fig. 1A. The formation of some non-agglomerated AuNRs was figured out which were mostly homogenous in terms of shape and size. The obtained AuNRs mean length was 50.0 ± 5.0 nm and mean width 12.0 nm. Fig 1B shows the optical absorption spectrum of AuNRs solution in the visible near IR region through which, two distinctive peaks at 530 and 808 nm are found. The longitudinal Plasmon mode results in higher energy (808 nm peak) and the transverse Plasmon mode results in lower energy (530 nm peak).

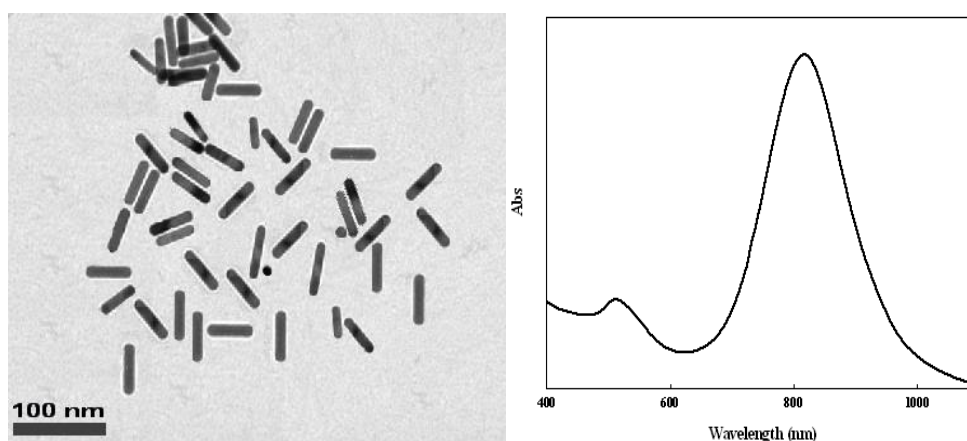


Figure 1: TEM images (A), and absorption spectra of aqueous of 50nm AuNRs solution (B).

Histopathological findings:

The examined section of prostate tissues of the control group showed apparent normal histomorphological structures (Fig.2 (A & B)).

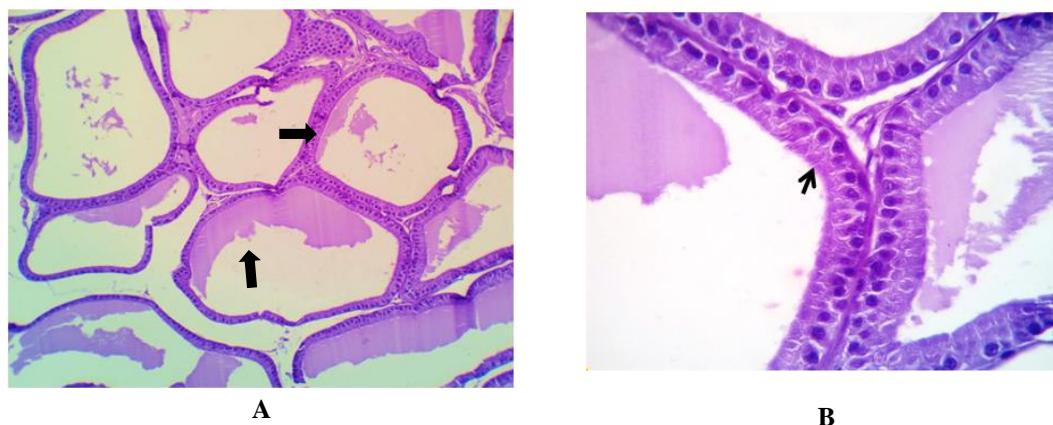


Figure 2: (A) Photomicrograph of the rats' prostate showing normal histomorphological structure (arrows). H & E x 200,
(B) High power showing normal epithelium of the rats' prostate gland (arrows). H & Ex400

On days 1 and 3 post-treatment, the prostate tissue structures were apparently normal with no significant abnormalities. Fig.3

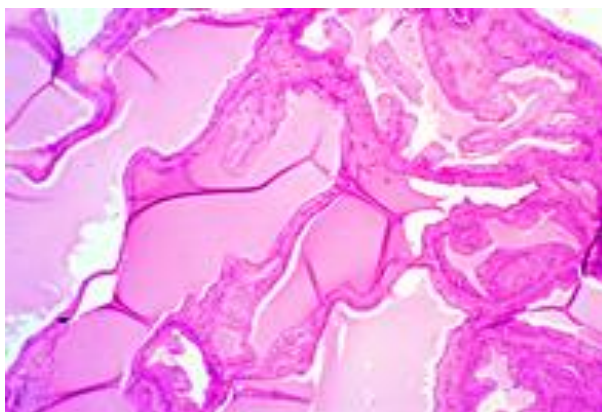


Figure 3: The examined sections from prostate revealed normal histomorphological structure

On day 7 post-treatment, the examined sections of prostate gland (*fig. 4, A*) revealed apparently normal prostatic tissue. Focal epithelial hyperplasia of some follicles was detected, but the sections on day 14 post-treatment showed normal acinar structures, matrix framework and secretory properties. A few acini showed mild cystic dilatation, focal or diffuse epithelial proliferation of the epithelial lining with double or triple layers, sometimes with papillary infolding. (Fig. 4, B)

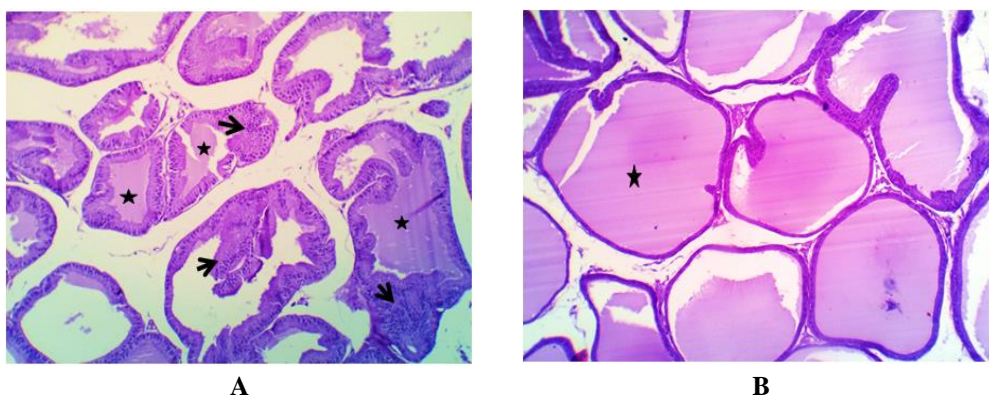


Figure 4: (A) Photo-micrograph of the rats' prostate gland showing apparently normal prostatic tissue with prostatic secretions (**stars**) and focal epithelial hyperplasia of some follicles (**arrows**). H&E X 400, (B) Photo-micrograph of the rats' Prostate gland showing mild cystic dilatation (**star**), focal epithelial hyperplasia and papillary infolding in some acini (**Arrows**).H&E X 200.

Electron microscopic findings:

Control group

The examined figures of electron microscope from different parts of control prostate gland revealed normal cellular arrangements of the main functional acinar and ductal compartments and normal stromal counterparts including the smooth muscle fibers, connective tissue cells, nerve fibers with their axons extensions, myoepithelial cells, interstitial tissue spaces beside blood vessel and vascular endothelial cells. The main acinar and ductal cells were seen in two main overviews, the glandular epithelial cells (prostatic ductal epithelial cells) with a tall columnar shape having elongated nucleus with two rounded edges and active dispersed chromatin with a clear nuclear membrane and normal size nucleolus. Such cells having their apical parts with their microvilli and the enriched pinocytotic membrane bounded vesicles open to the luminal side. The second cell type (Prostatic basal cells) showed polyhedral, oval or round nucleus having also active dispersed chromatin and normal nuclei, the cell membrane of these cells integrated to the basal lamina of the acini or ducts, with a little or inapparent pinocytotic vesicles. Both types of cells showed a main internal cytoplasmic features including nuclei with dispersed chromatin, interdigitations present between electron dense bodies, intercellular gaps, secretory vesicles of different shapes and sizes. The following figure displays rough endoplasmic reticulum, free

ribosomes, basal lamina cytoplasmic process of fibrocytes, pinocytic vesicles, Golgi apparatus, collagen fibers, bundle of filaments, hemidesmosome and nerve axon extension. (Fig.5)

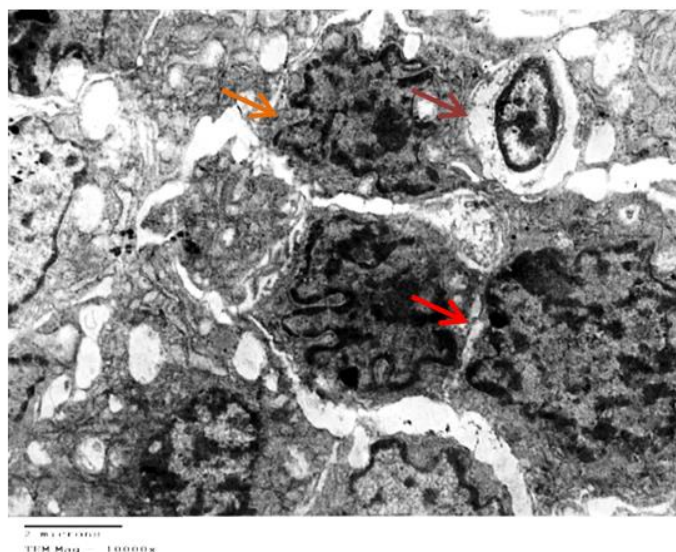


Figure 5: Electro-photo-micrograph of rat's prostate showing the basal lamina (blue arrow), basal cells (green arrow), myoepithelial cells (orange arrow), glandular epithelial cells (red arrow), intercellular gaps and digitations (yellow arrow) and secretory vesicles. X 5000, 10000.

The effect of intraperitoneal injection of 300 μ g/kg bwt gold nanorods on the prostate electron microscopy on days 1 and 3 post-treatment:

On day 1 post-treatment, the examined electron-micrographs revealed apoptotic changes in a variable number of the basal cells, where the nuclei appeared shrunken with a condensed fragmented or pitted nuclear membranes. Some nuclei showed blebbing of the nuclear membrane to form a new nucleosides repeats. The mitochondria, Golgi apparatus, RER, free ribosomes, secretory vesicles and electron dense bodies were diminished or depleted. In some micrographs, the surface microvilli appeared thick, stunted or denuded, the intended or shrunken nuclei with the blebbed nuclear membrane has been transformed to apoptotic bodies with dispersed nucleosides in the cytoplasm. The rough endoplasmic reticulum appeared swollen, distorted or disappeared. The mitochondria and other organelles were diminished or depleted and some of the secretory vesicles were distorted (Fig. 6A). After 3 days post-treatment, it was clear from figure 6B that the examined electro-micrograph of prostate tissue of this group revealed apoptotic changes in the nuclei of the basal cells with intended nuclear membranes, which appeared with more condensed and marginated nuclear chromatin. Some nuclei appeared greatly shrunken. The number of cytoplasmic organelles was very limited. The apical secretory vesicles were in a few numbers and mostly distorted. The microvilli were unapparent. Adjacent to the basal cells some myoepithelial cells and fibroblasts were seen. Distorted cellular interdigitating membranes with the basal lamina and blood capillaries in the interstitial tissue were also seen. Other micrographs showed rather degenerative reactions, where the apparently normal glandular epithelial cells were seen side by side to mildly shrunken nuclei or markedly pyknotic basal cell nuclei. In the degenerated cells, the mitochondria, RER, free ribosomes and the secretory vesicles were fewer in number with a lesser activities (distorted). The luminal microvilli were depleted. Still other sections showed apparently normal glandular epithelial cells and basal cells with normal distribution, numbers and arrangement of the cytoplasmic organelles.

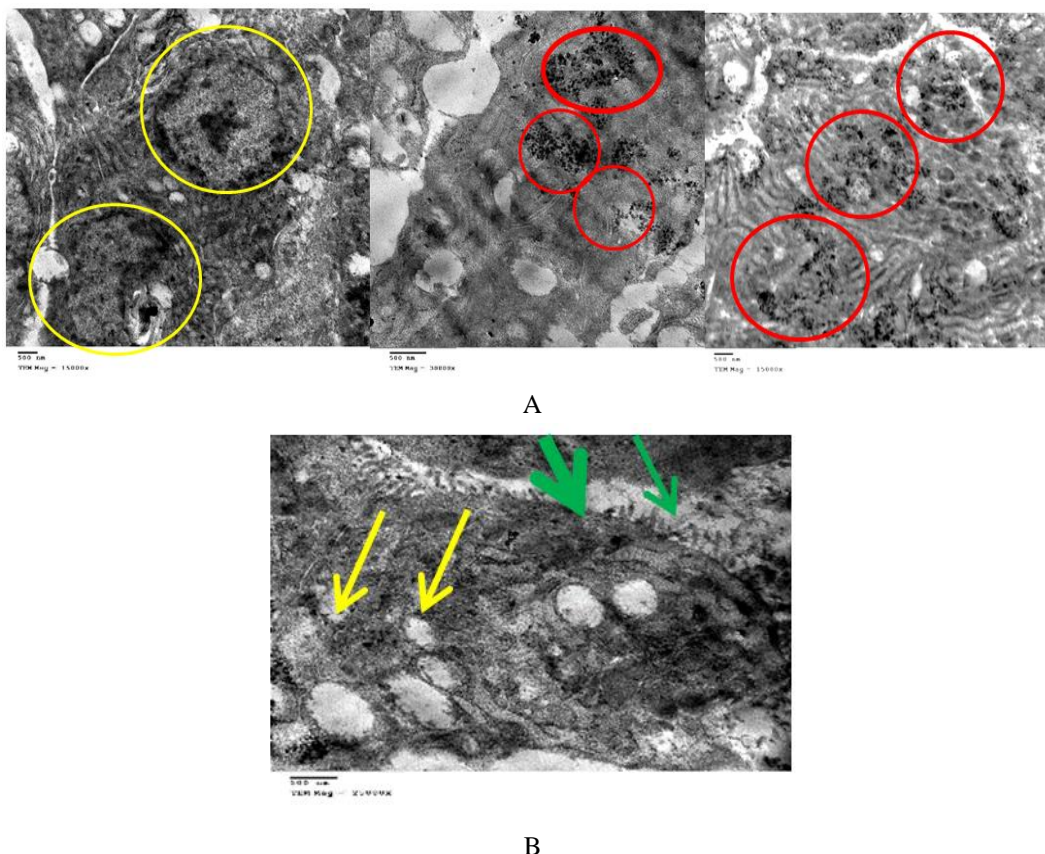


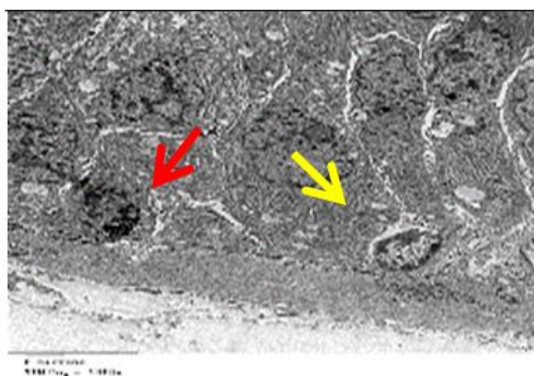
Figure 6: (A) Electro-photo micrograph of the rats' prostate showing the intended or shrunken nuclei with the blebbed nuclear membrane (yellow circles) transformed to apoptotic bodies with dispersed nucleosides in the cytoplasm (red circles). The rough endoplasmic reticulum appeared swelled distorted or disappeared. The mitochondria and other organelles were diminished or depleted.

(B) Electro-photo micrograph of the rats' prostate showing surface microvilli which appears thick, stunted or denuded (green arrow). The mitochondria and other organelles are diminished or depleted. Some of the secretory vesicles are distorted (yellow arrow). X 25000

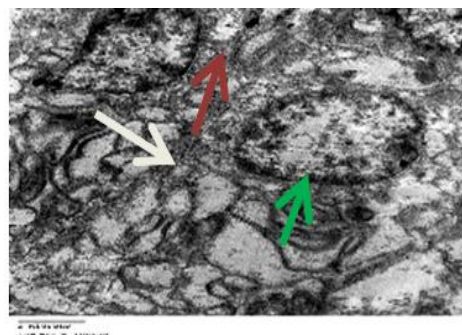
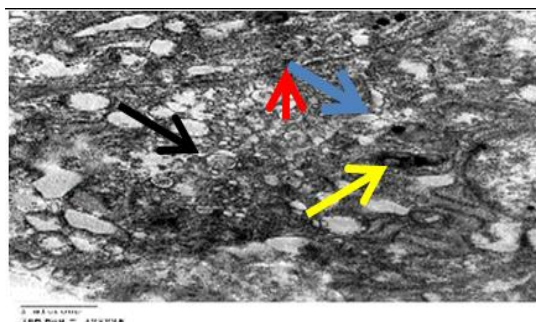
The effect of intraperitoneal injection of 300 μ g/kg bwt gold nanorods on the prostate electron microscopy on days 7 and 14 post-treatment:

Some of the examined electro-micrographs of this group revealed apparently normal prostatic glandular epithelial cells with elongated nuclei having normal regularly dispersed nuclear chromatin, nuclear membrane, intercellular gaps, RER, ribosomes, mitochondria, secretory vesicles, surface microvilli, luminal secretory products and corpora amylacia. Other micrographs showed many prostatic basal cells with a few of them suffering early apoptotic and early degenerative changes as represented by nuclear chromatin rearrangement or nuclear pyknosis. Other cytoplasmic organelles were apparently normal with presence of a few small secretory vesicles and a few electron dense bodies. (Fig. 7A)

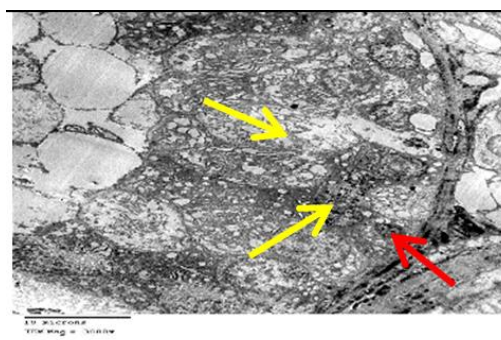
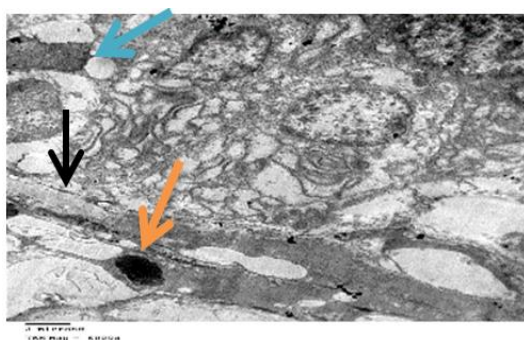
Some of the examined electro-micrographs of this group revealed apparently normal prostate cells with normal nuclear membrane, dispersed chromatin, which was more arranged around the nuclear membrane, mitochondria, RER, free ribosomes, interdigitating membranes and secretory vesicles containing the secretory granules, beside some phagolysosomes and electron dense bodies. Other micrographs showed the same organelle structures and distribution besides a large vesicle entangling granular and filamentous structures, rupture to the acinar lumen. Still other micrographs showed degenerative reactions represented by empty perinuclear halo space, pyknotic fragmented nucleus, besides a few unapparent cytoplasmic organelles and misconfigured, degenerated basal lamina. The interstitial tissue showed dilated spaces and a degenerated (pyknotic nucleus) cell (Figs.7B & 7C).



(A)



(B)



(C)

Figure 7 (A) Electro-photo micrograph of the rats' prostate showing many prostatic basal cells (blue arrow) with a few of them suffering early apoptotic (red arrow) and early degenerative changes as represented by nuclear chromatin rearrangement or nuclear pyknosis (yellow arrow). Other cytoplasmic organelles were apparently normal with presence of a few small secretory vesicles (green arrow) and a few electron dense bodies (brown arrow). X 10000, 5000

(B) Electro-photo micrograph of the rats' prostate showing apparently normal prostate cells with normal nuclear membrane, dispersed chromatin, which is more arranged around the nuclear membrane, mitochondria (green arrow), RER (orange arrow), free ribosomes (white arrow), interdigitating membranes (red arrow) and secretory vesicles containing the secretory granule (black arrow), beside some phagolysosome (yellow arrow) and electron dense bodies. (blue arrow) X 10000

(C) Electro-photo micrograph of the rats' prostate showing degenerative reactions represented by empty perinuclear halo space (blue arrow), pyknotic fragmented nucleus (yellow arrow), beside a few unapparent cytoplasmic organelles and disconfigurated, degenerated basal lamina (red arrow), dilated interstitial spaces (black arrow) with pyknotic nucleus (orange arrow).

DISCUSSION AND CONCLUSION:

In our study, the intraperitoneal injection of gold nanorods induced histopathologic and electron microscopic changes in prostate gland of male albino rats. Such changes were represented histopathologically (the prostate

revealed mild to moderate cystic dilatation with proliferation after 7 and 14 days post treatments, but no change occurred on day 1 and 3 post-treatment) and electro microscopically (the characteristic changes were represented by apoptotic changes and depletion of some materials especially RER, Golgi apparatus and cytoplasm).

In general, the GNP surface chemistry is an important factor that could determine apoptosis. Regarding the first day and third day post-treatment, the histopathological results revealed no structural or morphological abnormalities. The examined sections from prostate revealed normal histomorphological structure, this result is in agreement with Gormley et al. (2011), because they mentioned that the in vivo effect of RGDfK-gold nanorods for prostate cancer was not observed [9]. On day 7 and 14 post-treatment, the examined sections of Figure 4 revealed normal acinar structures, but a few acini showed mild cystic dilatation, focal or diffuse epithelial proliferation of the epithelial lining with double or triple layer. This cellular alteration could be due to the oxidant mechanism of GNRs by causing membrane destabilization ROS [10]. The epithelial proliferation that occurred may be due the positive charge of GNRs that enhance its interaction with the cell membrane [11]. Regarding the electron microscopic findings, the mentioned dose of GNRs caused mitochondrial disruption associated with apoptotic changes. In the same way, Schaublin et al. (2012) reported that long polyethylene glycol-gold nanorods induced disruption of the mitochondrial membrane potential and elicited apoptosis [12]. Also, our results are compatible with Huang et al. (2014) who illustrated that PEG-AuNPs induced a significant reduction in the mitochondrial transmembrane potential in K562 cells [13]. This indicates that PEG-AuNPs may affect the intrinsic apoptosis pathway. The mechanisms by which nanoparticle-induced cellular toxicity are largely due to several physical factors, especially i) the size of particle mobility across cell membranes [14]; (ii) high solubility that is different from that of its surface coating and particle composition; (iii) higher aggregation rate to enhance cellular bioaccumulation; (iv) interaction with biomolecules to form nanoparticle-protein complexes and DNA to alter cellular, physiological, and biochemical processes; and (v) the ability to generate abundant amounts of reactive oxygen species (ROS), which subsequently promote cellular injury by oxidative stress. Thus, the increased uptake of +ve charged nanoparticles may result in increased damage of the cellular membrane as well as increased damage of the cellular compartments like lysosomes [15]. Other factors affecting the cellular uptake of include ligand molecules that bind to specific cell membrane receptors induce apoptosis [16]. Regarding the 7th and 14th day post-treatment, it is clear that the prostatic tissue components started to return to their normal state. Lankveld et al. (2011) explained that the pegylated gold nanorods were almost cleared from the circulation after 2 days [17].

From this study it has been concluded that the injection of gold nanorods to male albino rats caused insignificant prostate tissue alterations as proved by histopathological findings. However, significant electron microscopic findings were observed. These findings indicated that gold nanorods can interact with prostate tissues. So, it is of interest to postulate that the study could be helpful in upcoming days to establish a concept on the role of gold nanorods in the management of cellular biological behaviors including prostate cancer and hyperplasia.

REFERENCES

1. Peer D, Karp JM, Hong S, Farokhzad OC, Margalit R, Langer R. Nanocarriers as an emerging platform for cancer therapy. *Nature nanotechnology*. 2007 Dec;2(12):751.
2. Astruc, D. Introduction to nanomedicine. *Molecules* 2016, 21, 4.
3. Rosenblum D, Joshi N, Tao W, Karp JM, Peer D. Progress and challenges towards targeted delivery of cancer therapeutics. *Nature communications*. 2018 Apr 12;9(1):1410.
4. Tiwari PM, Eroglu E, Bawage SS, Vig K, Miller ME, Pillai S, Dennis VA, Singh SR. Enhanced intracellular translocation and biodistribution of gold nanoparticles functionalized with a cell-penetrating peptide (VG-21) from vesicular stomatitis virus. *Biomaterials*. 2014 Nov 1;35(35):9484-94.
5. Riley RS, Day ES. Gold nanoparticle-mediated photothermal therapy: applications and opportunities for multimodal cancer treatment. *Wiley Interdisciplinary Reviews: Nanomedicine and Nanobiotechnology*. 2017 Jul;9(4):e1449.
6. Nikoobakht B, El-Sayed MA. Preparation and growth mechanism of gold nanorods (NRs) using seed-mediated growth method. *Chemistry of Materials*. 2003 May 20;15(10):1957-62.
7. Suvarnet, S., Layton, C. C., and John, D. B. Bancroft theory and practice of histological techniques, 7th edition, 2013.
8. Bozzola JJ. *Electron Microscopy*, 2nd Edition, 1999.

9. Gormley AJ, Malugin A, Ray A, Robinson R, Ghandehari H. Biological evaluation of RGDfK-gold nanorod conjugates for prostate cancer treatment. *Journal of drug targeting*. 2011 Dec 1;19(10):915-24.
10. Paviolo C, Haycock JW, Yong J, Yu A, Stoddart PR, McArthur SL. Laser exposure of gold nanorods can increase neuronal cell outgrowth. *Biotechnology and bioengineering*. 2013 Aug;110(8):2277-91. doi: 10.1002/bit.24889. Epub 2013 Mar 26.
11. Ito E, Yip KW, Katz D, Fonseca SB, Hedley DW, Chow S, Xu GW, Wood TE, Bastianutto C, Schimmer AD, Kelley SO. Potential use of cetrimonium bromide as an apoptosis-promoting anticancer agent for head and neck cancer. *Molecular pharmacology*. 2009 Nov 1;76(5):969-83.
12. Schaeublin NM, Braydich-Stolle LK, Maurer EI, Park K, MacCuspie RI, Afroz AN, Vaia RA, Saleh NB, Hussain SM. Does shape matter? Bioeffects of gold nanomaterials in a human skin cell model. *Langmuir*. 2012 Feb 3;28(6):3248-58.
13. Huang YC, Yang YC, Yang KC, Shieh HR, Wang TY, Hwu Y, Chen YJ. Pegylated gold nanoparticles induce apoptosis in human chronic myeloid leukemia cells. *BioMed research international*. 2014;2014.
14. Lynch I, Cedervall T, Lundqvist M, Cabaleiro-Lago C, Linse S, Dawson KA. The nanoparticle–protein complex as a biological entity; a complex fluids and surface science challenge for the 21st century. *Advances in colloid and interface science*. 2007 Oct 31;134:167-74.
15. Xia T, Kovochich M, Brant J, Hotze M, Sempf J, Oberley T, Sioutas C, Yeh JI, Wiesner MR, Nel AE. Comparison of the abilities of ambient and manufactured nanoparticles to induce cellular toxicity according to an oxidative stress paradigm. *Nano letters*. 2006 Aug 9;6(8):1794-807. doi: 10.1021/nl061025k
16. Nel AE, Mädler L, Velegol D, Xia T, Hoek EM, Somasundaran P, Klaessig F, Castranova V, Thompson M. Understanding biophysicochemical interactions at the nano–bio interface. *Nature materials*. 2009 Jul;8(7):543. doi: 10.1038/nmat2442
17. Lankveld DP, Rayavarapu RG, Krystek P, Oomen AG, Verharen HW, Van Leeuwen TG, De Jong WH, Manohar S. Blood clearance and tissue distribution of PEGylated and non-PEGylated gold nanorods after intravenous administration in rats. *Nanomedicine*. 2011 Feb;6(2):339-49.